IOP Publishing Physica Scripta
Phys. Scr. 95 (2020) 065505 (9pp) https://doi.org/10.1088/1402-4896/ab7f49

# Metamaterials absorber for multiple frequency points within 1 GHz

**Jing Wang[1], Xiaoxia Ding[1], Xiaojun Huang[2], Jiong Wu[1], Yujun Li[1] and Helin Yang[1]**

[1] College of Physical Science and Technology, Central China Normal University, Wuhan 430079, People's Republic of China
[2] College of Communication and Information Engineering, Xi'an University of Science and Technology, Xi'an 710054, People's Republic of China

E-mail: emyang@mail.ccnu.edu.cn

Received 10 January 2020, revised 8 March 2020
Accepted for publication 12 March 2020
Published 2 April 2020

**Abstract**

Designing high efficiency microwave absorbers with frequencies in 1 GHz is still a huge challenge in practical applications. We design and present a novel microwave metamaterials absorber at six frequency points of 160, 442, 530, 723, 765 and 965 MHz with absorptances up to 90%, which is insensitive to polarization, viable at wide incidence angle and relatively simple in structure. We demonstrate the absorption characteristics of the absorber and explain the mechanism by means of equivalent impedance theory, surface current and energy distribution. The experimental results verify the correctness of the simulation and provide valuable reference for the design of broad-band microwave absorber in lower frequency band.

Keywords: metamaterials, low frequency, absorber, multiple frequency

(Some figures may appear in colour only in the online journal)

## 1. Introduction

Artificial composite matematerials(MMs), which are precisely arranged of block constructions whose unit size are small compared with the incident electromagnetic (EM) wave. The effective permittivity ($\varepsilon_{eff}$) and effective permeability ($\mu_{eff}$) of the MMs are manual-controlled and have ordinary physical properties that are not found in natural materials, such as negative refractive index [1, 2], slow light [3–5], super resolutions [6, 7] and invisibility cloaking [8, 9]. Giving the credit to its satisfactory properties, MMs have attracted attention of many researchers in recent decades and been used in wide range from radio [10], microwave [11], THz [12], infrared [13] to visible [14].

Since the perfect metamaterial absorber has been put forward in 2008 by N I Landy [15] who had laid a solid foundation for future generations, MMA broke through the limitation of the traditional absorber and occupied the sights of the researchers as an crucial embranchment of MMs application. Thus, MMA has been applied to solar cell [16], amplifiers [17], radomes [18], sensors [19], switches and etc. In terms of MMA, controlling the impedance of the MMA by changing the real and imaginary parts of the $\varepsilon_{eff}$ and the $\mu_{eff}$ enables $Z_{eff} = \sqrt{\mu_{eff}/\varepsilon_{eff}}$ to faultlessly match with the free space and thus reduce reflection. EM energy can be ideally consumed by MMA in its interior by reducing reflection and transmission.

Since the rise of MMA, absorbers for different frequency ranges have been developed by a great many researchers in different forms [20–22]. Researchers proposed a compact quad-band polarization independent metamaterial absorber which has four absorption peaks at 3.1 GHz, 5.5 GHz, 7.6 GHz and 10.98 GHz [23]. A perfect absorber with polarization insensitive peaks at 7 GHz and 15 GHz also has been proposed [24]. Due to the relatively narrow range of applications of absorbers with individual absorption peak and the inability to broaden the frequency band also being one of the disadvantages of MMs, researchers have begun to focus on the development of ultrawide-band absorbers [25, 26]. Thus a broadband absorber used the simplified multireflection interference theory to analyze an ultra-broadband metamaterial absorber appeared and the ultra-wideband water-based

 

metamaterial absorber came across, which provides 90% absorptance in the frequency range of 7.9–21.7 GHz stably at different temperatures [27, 28]. Besides absorbers in frequency of GHz band, researchers also employed two-dimensional carbon nanotube materials graphene owing excellent properties of optical and electrical mechanisms to throw up a number of THz spectrum absorbers, such as some graphene-based THz absorbers whose absorptance can reach 90% and a tunable polarization insensitive ultra-broadband absorber based on the plasma metamaterial [29, 30]. In addition, some magnetic materials-based absorbers such as the Ferrite-based metamaterial microwave absorber with absorption frequency magnetically tunable in a wide range also appeared one after another [31, 32]. However, scanning the research history and current status of MMA, designing low frequency absorber is a rather difficult problem to solve and a very hot topic. Therefore, it is a significant and arduous task to complete an absorber at low frequency.

Researchers designed a dual/triple-band metamaterial absorber at very low frequency which have two absorption peaks at 305 and 360.5 MHz, respectively [33]. However, the MMA they designed used lumped components, which made the process relatively complicated and the ratio of unit size to wavelength was $a/\lambda = 1/1.5$. They also designed an metamaterial absorber with a single absorption peak at 440 MHz, whose unit size is about $1\lambda$ [34]. There is also a low-frequency perfect sandwich meta-absorber which has single absorption peak at 404 MHz and the length of its periodic unit cell is 82.5 mm [35]. Another low-frequency metamaterial absorber based on corrugated surface have a length of 45 mm and an absorption peak at 362 MHz [36]. It can be noticed that researchers attach great importance to the dig of EM applications at low frequency to conquer the shortcomings like large size and complex structure and so on.

In this paper, we introduce the MMA with multi-frequency points within 1 GHz with a relatively small unit structure. The lowest frequency of the absorber we designed can reach 160 MHz whose unit side length is $1/14\lambda$. We elucidate the mechanism of the absorption of the MMA and manufacture the experimental samples by the method of PCB (Printed Circuit Board).

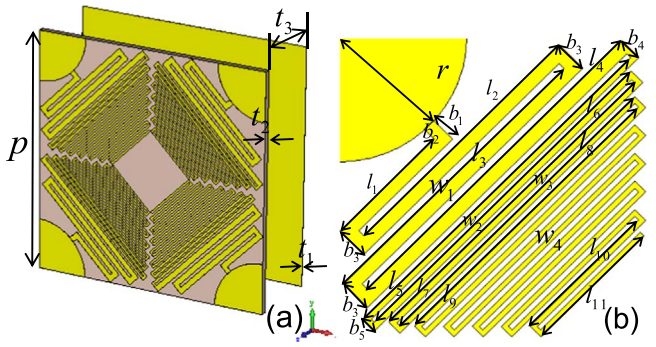


**Figure 1.** (a) Perspective views of the unit cell structure. (b) One quarter of the photograph of the structure.

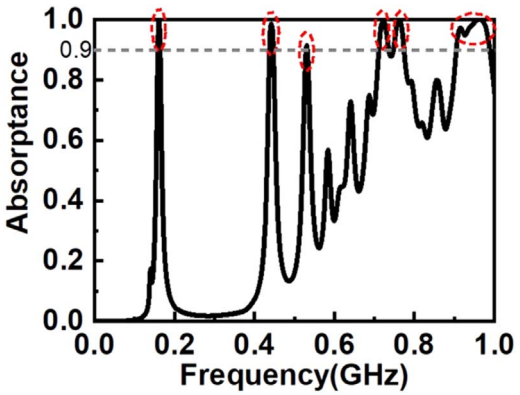


**Figure 2.** Absorptance simulation results of the absorber within 1 GHz.

**Table 1.** The geometric parameters of the unit cell structure.

| $r$ | $b_1$ | $b_2$ | $b_3$ | $b_4$ | $b_5$ |
|---|---|---|---|---|---|
| 25.0 | 5.3 | 2.7 | 6.6 | 4.9 | 3.1 |
| $l_1$ | $l_2$ | $l_3$ | $l_4$ | $l_5$ | $l_6$ |
| 26.0 | 54.0 | 61.0 | 70.3 | 74.0 | 71.0 |
| $l_7$ | $l_8$ | $l_9$ | $l_{10}$ | $l_{11}$ | $w_1$ |
| 67.9 | 65.0 | 62.0 | 30.0 | 27.5 | 2.6 |
| $w_2$ | $w_3$ | $w_4$ | unit | | |
| 1.2 | 1.1 | 1 | mm | | |

## 2. Design and simulation

The three-dimensional unit cell of the MMA is presented in figure 1(a). The proposed unit cell MMA be composed of four layers. The front metallic-pattern layer and the bottom metal layer have a conductivity of $\sigma = 5.8 \times 10^7\ \mathrm{S\ m^{-1}}$ and thickness of $t_1 = 0.035$ mm. The second layer has a thickness of $t_2 = 3$ mm,which employed the FR4 with a dielectric constant of 4.3 and a loss angle of 0.025 and it is separated from the bottom layer by the third air layer with thickness of $t_3 = 38$ mm. Figure 1(b) shows the geometry of one piece that rotate into four pieces to compose the metallic-pattern layer of the MMA. The radius $r$ of the quarter circle and the geometric parameters of the rectangular strip are listed in table 1 and all values are measured in mm. The short and the long sides of the rectangular bar are $b$ and $l$ respectively. All the short edges after $b_5$ have the same value as $b_5$. The values of long sides from $l_9$ to $l_{10}$ are the arithmetic progressions with tolerances of four. From $l_1$ to $l_4$, $l_5$ to $l_6$, $l_7$ to $l_8$ and $l_9$ to $l_{10}$, four kinds of metal strips with width of $w_1$, $w_2$, $w_3$ and $w_4$ were used in MMA designing respectively. Bending the square loop inward extends the surface area to increase the inductance $L$ and capacitance $C$. Increasing $L$ and $C$ enables $f$ to become small based on the equation of $f = 1/(2\pi\sqrt{LC})$.

The proposed MMA was designed and simulated by CST Microwave Studio which is based on the finite integral method. In the simulation, the boundary condition was set to be unit cell and open (add space) in the $x$, $y$ and $z$ direction, respectively. Since the transmittance can be regarded as zero because of the bottom layer, the equation $A(\omega) = 1 - |S_{11}|^2$

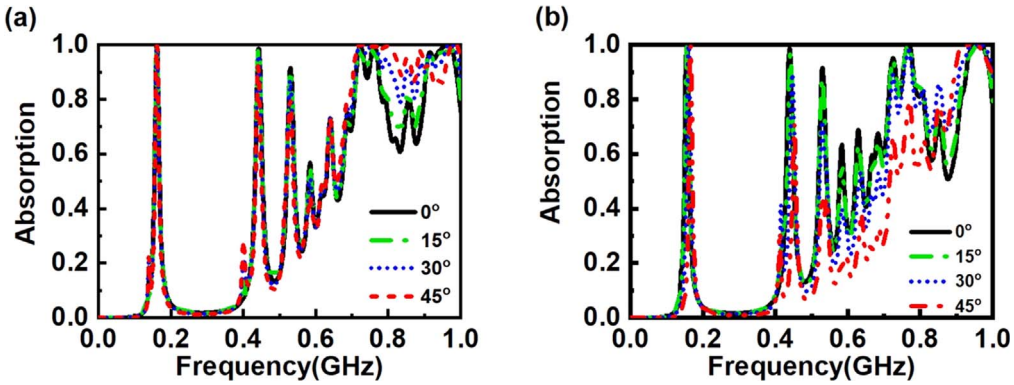


**Figure 3.** Simulated results of absorption of MMA in different incident angles: (a) TE mode. (b) TM mode.

can be used to calculate the absorptance, where $A(\omega)$ and $S_{11}$ represent absorptance and reflectance, respectively.

The simulation results of the absorption of the MMA proposed within the frequency of 1 GHz are shown in figure 2. The MMA achieved the target to bring forth multiple absorption peaks in the frequency range within 1 GHz, and the lowest frequency is as low as 160 MHz whose length of the unit cell can reach $\lambda/14$. The absorptance was 99.5% at 160 MHz, 98.6% at 442 MHz, 91.6% at 530 MHz, followed by three absorption peaks with broadband absorption effect, 99.4% at 723 MHz, 99.2% at 765 MHz, and 97.2% of the last absorption point at 965 MHz.

Based on the data above, we only analyzed the absorption characteristics of the absorber in the case of normal incidence of EM waves. In order to conform to the actual circumstances, it is necessary to analyze the absorption performance of the absorber when EM wave is incident at different angles. Thus, as is shown in figure 3, we analyzed the absorption in TE and TM modes of the absorber respectively in the range of incidence angle from 0° to 45°. From the simulation results of TE wave in the figure 3(a), it can be seen that the change of incident angle at the frequency point of 160 MHz has little influence on the absorption performance. At the second absorption peak there is little shift in frequency and an easing in absorption in the course of the change in incident angle. At the frequency of 530 MHz, the absorption trend of the absorber at different EM incidence angles is roughly the same as the trend of the previous absorption peak. From 723 to 965 MHz, with the increase of incident wave angle, the absorption presented an upward trend and gradually evolved from independent absorption frequency points to a small band of broadband absorption. In TE mode, the absorber we designed performs very well in the case of wide incident angle and even appears to be more favorable than normal incidence.

For the sake of delving into the operation rules of MMA in different modes, we also conducted an in-depth analysis of MMA in TM mode from 0° to 45° in figure 3(b). Similar to the case in TE mode, the change in angle has very little effect on absorption and frequency at the lowest frequency point. The absorption reduction and the blue shift at the second frequency point are rather trifling and the absorptance still remains above 85%, which means that in this mode the MMA

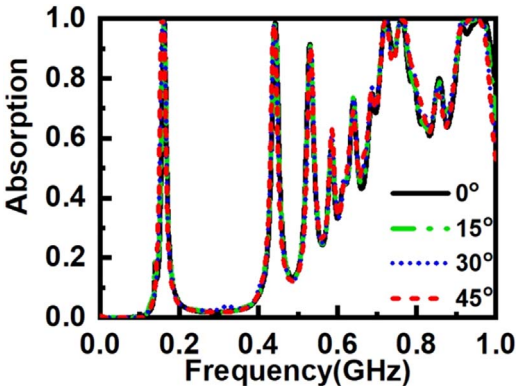


**Figure 4.** Simulation results of absorption in different polarization angle.

is slightly worse only at 45°. The third frequency point is confirmed to be much same with the previous frequency point except that there was no significant frequency shift. From the figure, it can be seen that the three waveforms we got from 0° to 45° after 700 MHz almost all overlapped and there was only a certain absorption reduction at 45°.

Although we designed MMA to be completely symmetric, whether it possess the characteristics of polarization insensitivity needs to be verified likewise. Figure 4 is the simulation results of absorption with polarization angle varying from 0° to 45°. The diagrams demonstrated in the figure indicated that all the graphs are almost coincident, which manifested that the absorption performance of the MMA is almost unchanged in the wake of altering of polarization angle. This verified that the absorber is polarization-insensitive.

## 3. Discussions and experiments

In order to further analyze MMA from the perspective of essential current flow direction and state, we displayed the simulation results of surface current at six major absorption peaks within 1 GHz in figure 5. Firstly, in figure 5(a) the surface current distribution and flow direction at 160 MHz and 442 MHz are very similar. The current at these two frequency points is mainly distributed on a large area of the strip

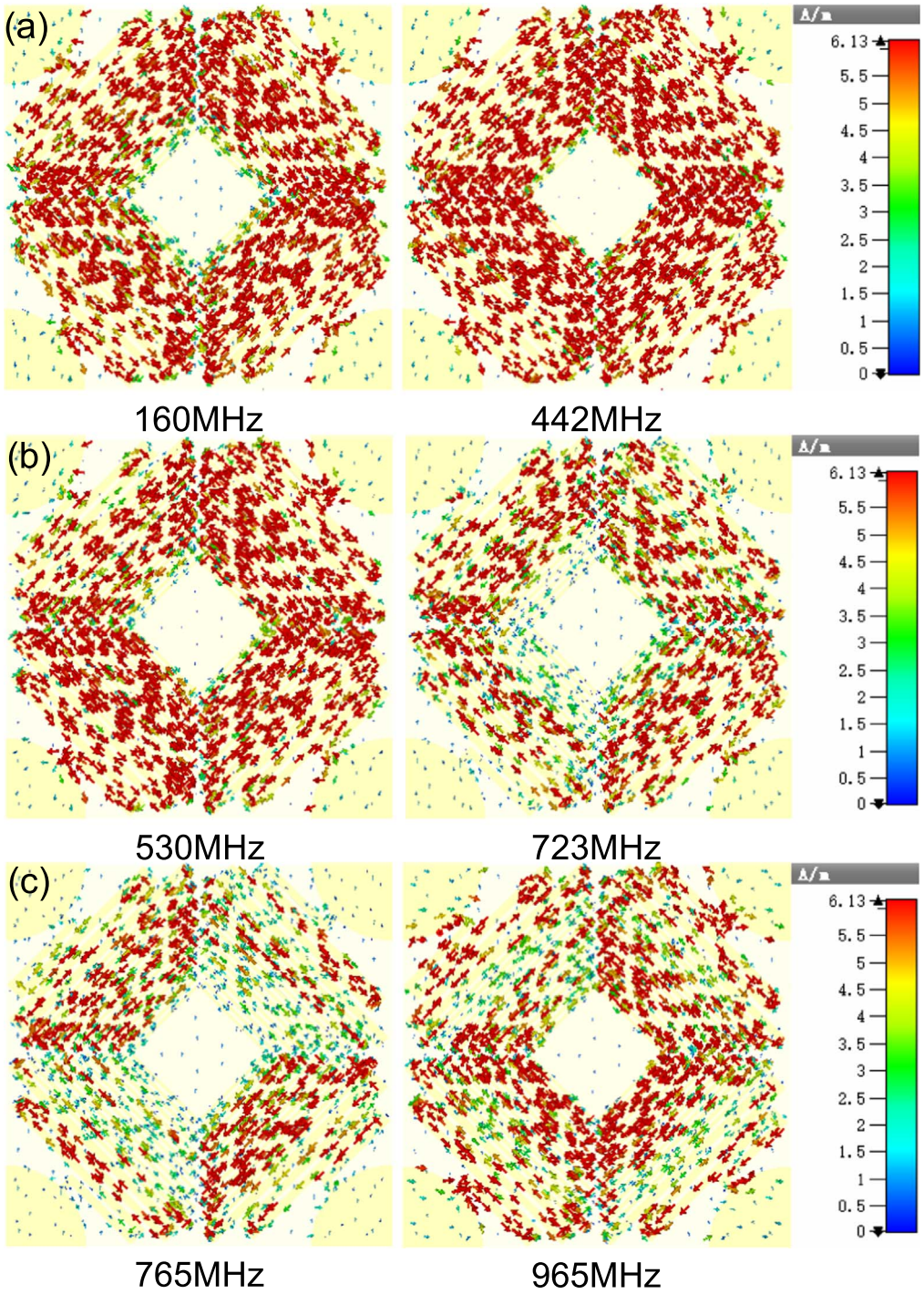


**Figure 5.** Surface current at six major absorption peaks:(a) 160 and 442 MHz. (b) 530 and 723 MHz. (c) 765 and 965 MHz.

loop and extends inward along the direction and edge of the strip loop, starting from the junction of the outermost strip loop and the quarter loop. The difference between them is that the surface current at 160 MHz mainly distributed along the edge of the square bar at the middle position while the surface current at 442 MHz is principally circulated down the edge of the inner square bar, and the surface current distribution at 442 MHz is denser. The surface current performance at 530 MHz is actually about the same as that at 160 MHz except that it is more evenly distributed across the various stripes at 160 MHz. As can be seen from the figures 5(b) and (c), the surface currents of two frequency points at 723 and 765 MHz start to decrease and mainly distributed in the middle part of the strip rings. Regarding the center of the unit cell as the origin, the surface currents are more inclined to flow at the edges of the strip ring in the second and fourth quadrants. And at 765 MHz, what's different from all the other points is that the current is flowing in the opposite direction to all the other frequency points. In figure 5(c), the current distribution at 965 MHz is mainly distributed at the

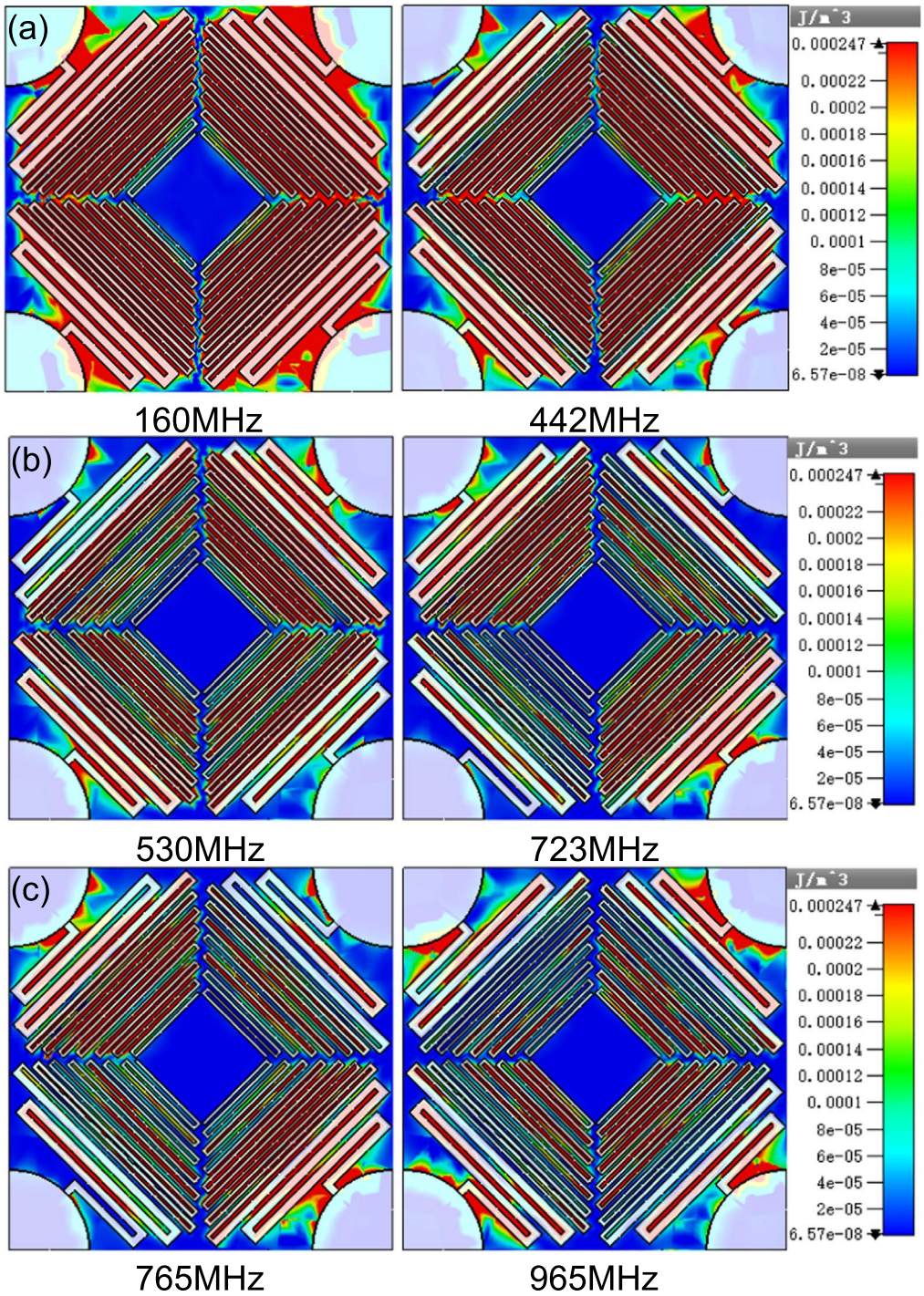


**Figure 6.** Magnetic energy distribution of six main absorption peaks: (a) 160 and 442 MHz. (b) 530 and 723 MHz. (c) 765 and 965 MHz.

edge of the quarter disk and the central part of the strip rings. From the research of surface current, it can be seen that the existence of a central strip loop causes the current to flow in a '*z*' shape, thus the increasing current flow path can reach the goal of making the frequency move towards a lower direction. Owing to this, the MMA is able to accomplish the task with a relatively small size compare with the absorbed EM wave at low frequency.

Due to the absorption effect induced by magnetic resonance, we followed up with an in-depth study on the magnetic energy distribution of the same six main absorption peaks. It can be seen from figure 6 that the magnetic energy distribution at these six frequency points is basically consistent with their surface current distribution. In figure 6(a) the magnetic energy at 160 and 442 MHz is strongly distributed around the metal, while at 530 MHz it begins to decay significantly. Because the two frequency points 723 and 765 MHz are close to each other, the magnetic energy distributions displayed are almost the same according to figures 6(b) and (c). The 965 MHz magnetic energy is gathered at the connection

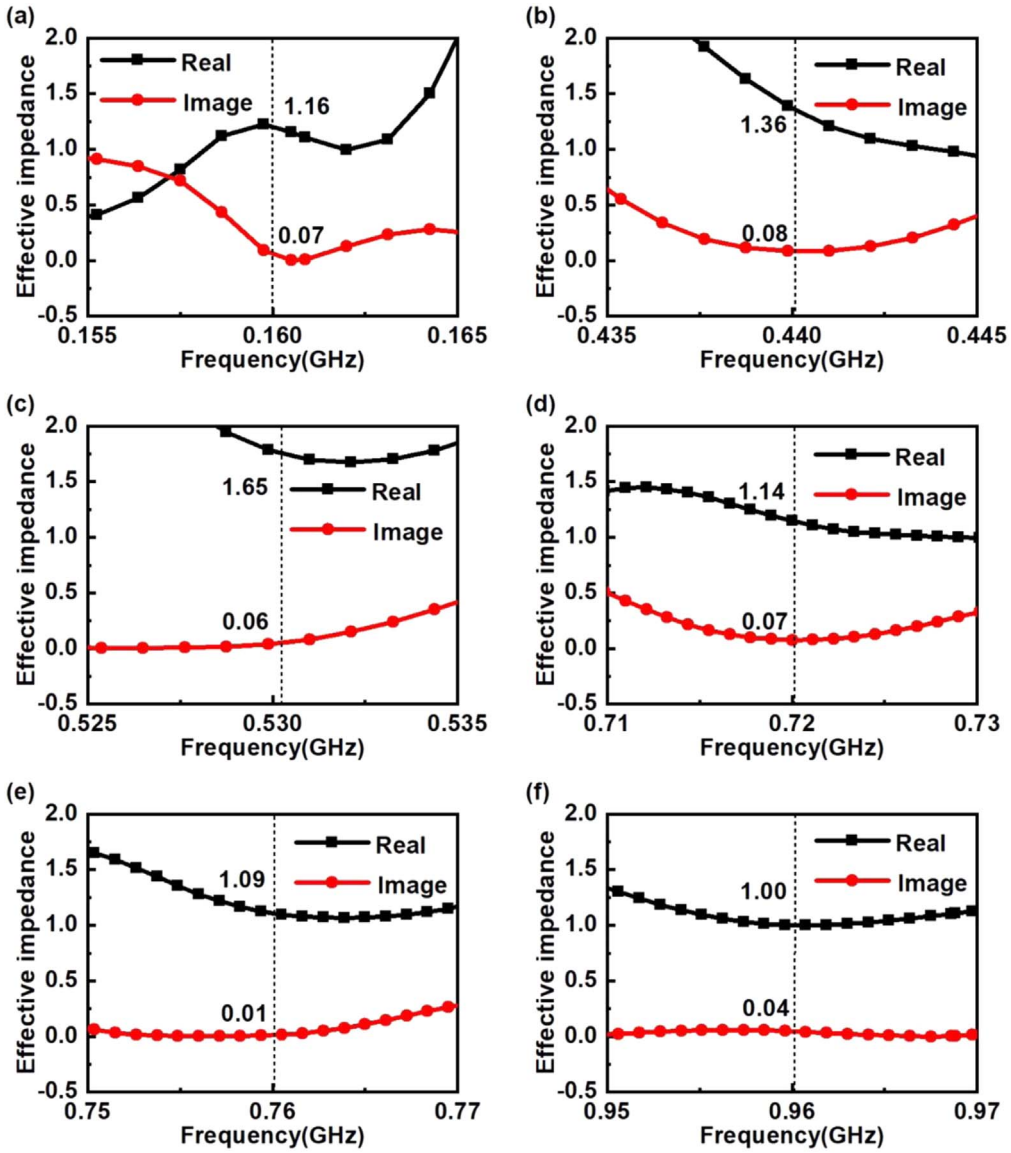


**Figure 7.** The equivalent impedance matching results $Z_{eff}$ of MMA: (a) 160 MHz. (b) 442 MHz. (c) 530 MHz.(d) 723 MHz. (e) 765 MHz. (f) 965 MHz.

between the quarter disk and the strip. It is proved that the absorbing effect generated from the magnetic resonance according to the analysis of surface current and the verification of magnetic energy distribution.

We also analyze the absorber based on the traditional impedance matching theory. S-parameters are extracted from CST and utilized for impedance matching formula $Z_{eff} = \sqrt{\frac{(1+S_{11})^2}{(1-S_{11})^2}}$. The equivalent impedance matching results of the six absorption peaks are obtained from the above formula and the specific values of the real and the imaginary part are shown in figure 7. At 160, 442, 723, 765 and 965 MHz, the real parts of the equivalent impedance are approximately equal to 1 when imaginary parts are around 0. The absorber keeps a good impedance match with the free space at these frequency points and most energy is consumed in the absorber to achieve efficient absorption. It can also be seen from the figure that the closer the value of the real part is to 1, the higher the absorptance of the frequency point will be. Among them, in figure 7(c) the matching value of real part equivalent impedance at 530 MHz slightly deviates from the value 1, indicating that its absorption is slightly weaker. The disciplines of equivalent impedance curves are consistent with the results of absorption frequency points, which shows that the equivalent impedance obtained by parameter inversion is correct.

The $S_{11}$ parameters of the designed absorber are measured experimentally. In figure 8(a) we used a pair of broadband horn antennas of model number OBH460, a vector network analyzer of model number Agilent E8362B and a square sample with a side length of 600 mm to get the reflectance. The MMA with metal substrate is placed in front of two horn antennas with a small angle around $\theta = 6°$ to the horizontal plane, one of which is used for receiving signals and the other for transmitting signals. When placing experimental equipment, the distance between the sample and the

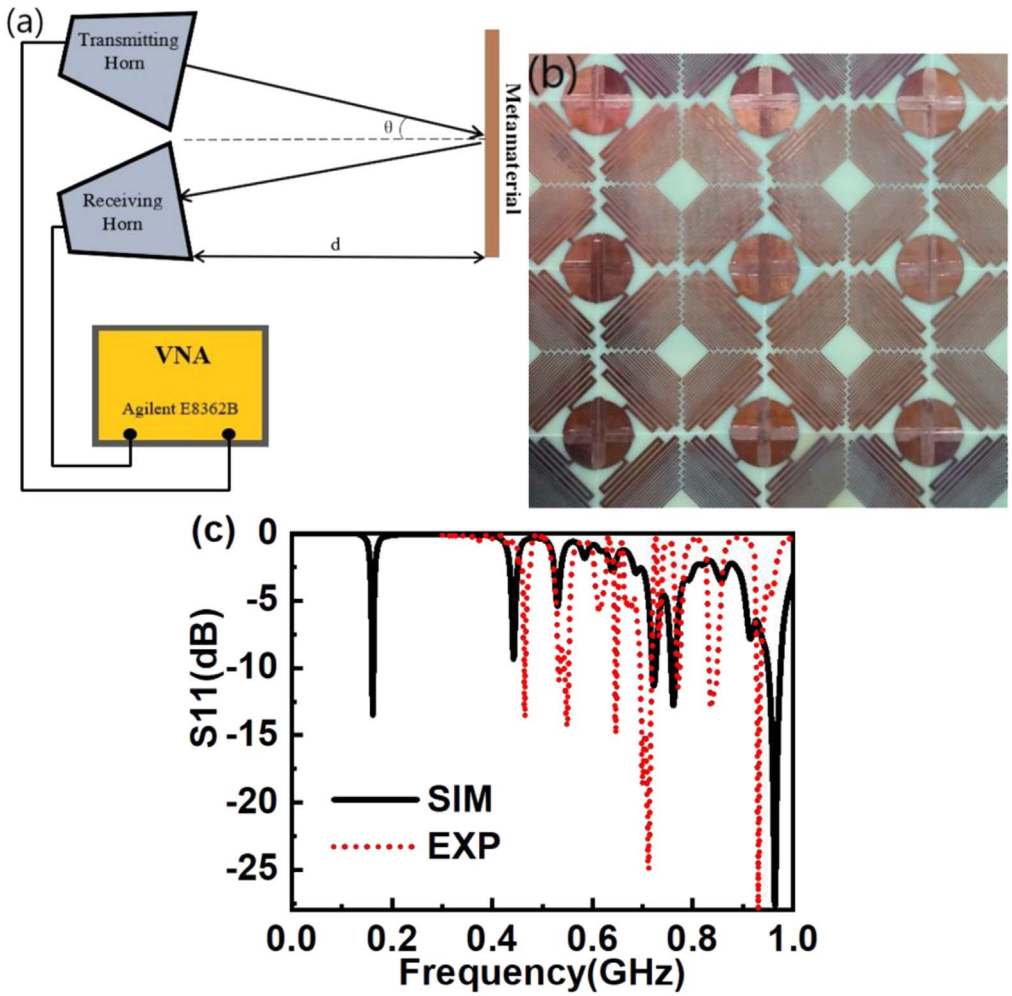


**Figure 8.** (a) Schematic diagram of experiment settings. (b) Part of the measured sample. (c) The comparison between experimental and simulation result of the S-parameter of the absorber.

antenna horn met the far field conditions is $d = 3m$ . The horn antenna and the vector network analyzer are connected through the coaxial line to complete the signal transmission and reception as well as data processing so as to calculate the reflection of the absorber. In figure 8(b), we present a part of the measured sample. Due to the rigorous requirements of low-frequency experiments and the fact that low-frequency absorbers are highly susceptible to the external environment, the experimental results we can provide are exceedingly confined. Figure 8(c) is the experimental result of the $S_{11}$ of the absorber. Since the horn antennas used for measurement ranging from 400 MHz to 6 GHz, we can only give the test results above 400 MHz. It can be seen from figure 8(c) that there is an absorption peak at 450 MHz, whose result is basically consistent with that at 440 MHz in the simulation results, but with a certain blue shift. In the experiment, the result almost corresponds to the simulation result except for a certain increase in absorption at 530 MHz. For the absorption peaks described above, compared with the simulation results, the absorption of the experimental results increased in different degrees. In the figure of experimental results, a relatively obvious absorption occurs at 640 MHz. Based on the situation of other frequency points, it can be basically identified as a smaller absorption peak at 640 MHz in the simulation. There are two absorption peaks between 700 MHz and 800 MHz, which basically correspond to the results at 723 MHz and 765 MHz in the simulation. The absorption peak at 840 MHz is the same as the result at 640 MHz. In the simulation results, there is also a small absorption peak at 840 MHz but the absorption is enhanced in experiment so this absorption result occurs. The absorption peak at 930 MHz also corresponds to the frequency point at 965 MHz in the simulation results. According to the above comparison between simulation and experimental results, it can be seen that each absorption peak in the simulation has its corresponding absorption frequency point and absorption effect in the experimental results. Although the matching degree of the two waveforms is not particularly high, experimental results can still be used as the proof of the correctness of the simulation results.

In that the low frequency experiment has very strict requirements and the EM wave is very sensitive, which means it is easy to be fluctuated due to external interference, there are certain differences between the experimented and the simulated results. The dielectric constant of FR-4 in simulation is 4.3, but the dielectric parameter of the tested material

might not be 4.3. The difference between the materials used in the experiment and the simulation may result in the frequency shift of the frequency points. In addition to the limited manufacturing accuracy, uneven surface, rough edges of MMA sample and the coupling effect between the horn antenna used in the experiment resulted in some deviations between our experimental results and the simulation results, but experimental results verify the correctness of the simulation.

## 4. Conclusion

We proposed a low frequency absorber with multiple absorption frequency points within 1 GHz, which is insensitive to polarization and has better absorption performance under the condition of wide incidence angle. We explain the mechanism of these absorption formation from the aspects of surface current, magnetic energy distribution and impedance matching and verify the simulation results with the experimental results, which are roughly consistent with the simulation results. Therefore, the MMA has broad application prospects in electromagnetic shielding and other fields.

## Acknowledgments

This work was supported by the National Natural Science Foundation of China (No. 61701206), and by the Fundamental Research Funds for the Central Universities (innovation funding project) (No. 2019CXZZ099, 2019CXZZ103).

## ORCID iDs

Helin Yang https://orcid.org/0000-0002-1107-9557

## References

[1] Cheng D, Chen H, Zhang N, Zhang H, Xie J and Deng L 2013 Numerical study of a dualband negative index material with polarization independence in the middle infrared regime *J. Opt. Soc. Am.* B **30** 224-228
[2] Gao L, Shigeta K, Vazquez-Guardado A, Progler C J, Bogart G R, Rogers J A and Chanda D 2014 Nanoimprinting techniques for large-area three-dimensional negative index metamaterials with operation in the visible and telecom bands *ACS Nano* **8** 5535-5542
[3] Mousavi S H, Khanikaev A B, Allen J, Allen M and Shvets G 2014 Gyromagnetically induced transparency of metasurfaces *Phys. Rev. Lett.* **112** 1-6
[4] Jang M S and Atwater H 2011 Plasmonic rainbow trapping structures for light localization and spectrum splitting *Phys. Rev. Lett.* **107** 1-5
[5] Thuy V T T, Tung N T, Park J W, Lam V D, Lee Y P and Rhee J Y 2010 Highly dispersive transparency in coupled metamaterials *J. Opt.* **12** 1-7
[6] Scarborough C P, Jiang Z H, Werner D H, Rivero-Baleine C and Drake C 2012 Experimental demonstration of an isotropic metamaterial super lens with negative unity permeability at 8.5 MHz *Appl. Phys. Lett.* **101** 99-102
[7] Nicholas F, Hyesog L, Cheng S and Xiang Z 2005 Sub-Diffraction-Limited Optical Imaging with a Silver Superlens *Science* **308** 534-537
[8] Schurig D, Mock J J, Justice B J, Cummer S A, Pendry J B, Starr A F and Smith D R 2006 Metamaterial electromagnetic cloak at microwave frequencies *Science* **314** 977-980
[9] Pawlik G, Tarnowski K, Walasik W, Mitus A C and Khoo I C 2012 Infrared cylindrical cloak in nanosphere dispersed liquid crystal metamaterial *Opt. Lett.* **37** 1847-1849
[10] Wiltshire A M C K, Pendry J B, Young I R, Larkman D J, Gilderdale D J and Hajnal J V 2016 Microstructured Magnetic Materials for RF Flux Guides in Magnetic Resonance Imaging *Science* **291** 849-851
[11] Lam V D, Kim J B, Lee S J and Lee Y P 2008 Left-handed behavior of combined and fishnet structures *J. Appl. Phys.* **103** 3–7
[12] Bui S T, Nguyen V D, Bui X K, Nguyen T T, Lievens P, Lee Y and Vu D L 2013 Thermally tunable magnetic metamaterials at THz frequencies *J. Opt. (United Kingdom)* **15** 11–16
[13] Rockstuhl C, Zentgraf T, Guo H, Liu N, Etrich C, Loa I, Syassen K, Kuhl J, Lederer F and Giessen H 2006 Resonances of split-ring resonator metamaterials in the near infrared *Appl. Phys. B Lasers Opt.* **84** 219–227
[14] Yao J, Liu Z, Liu Y, Wang Y, Sun C, Bartal G, Stacy A M and Zhang X 2008 Optical negative refraction in bulk metamaterials of nanowires *Science* **321** 930
[15] Landy N I, Sajuyigbe S, Mock J J, Smith D R and Padilla W J 2008 Perfect metamaterial absorber *Phys. Rev. Lett.* **100** 207402
[16] Hamm J M, Sebastian W, Tsakmakidis K T and Ortwin H 2011 Theory of Light Amplification in Active Fishnet Metamaterials *Phys. Rev. Lett.* **107** 167405
[17] Castellanos-Beltran M A, Irwin K D, Hilton G C, Vale L R and Lehnert K W 2008 Amplification and squeezing of quantum noise with a tunable Josephson metamaterial *Nat. Phys.* **4** 928–931
[18] Jiang T, Wang Z, Li D, Pan J, Zhang B, Huangfu J, Salamin Y, Li C and Ran L 2012 Low-DC voltage-controlled steering-antenna radome utilizing tunable active metamaterial *IEEE Trans. Microw. Theory Tech.* **60** 170–178
[19] Li Y B, Li L L, Xu B B, Wu W, Wu R Y, Wan X, Cheng Q and Cui T J 2016 Transmission-Type 2-Bit Programmable Metasurface for Single-Sensor and Single-Frequency Microwave Imaging *Sci. Rep.* **6** 23731
[20] Mao Z, Liu S, Bian B, Wang B, Ma B, Chen L and Xu J 2014 Multi-band polarization-insensitive metamaterial absorber based on Chinese ancient coin-shaped structures *J. Appl. Phys.* **115** 204505
[21] Li L Y, Wang J, Du H L, Wang J F and Qu S B 2015 Achieving a multi-band metamaterial perfect absorber via a hexagonal ring dielectric resonator *Chinese Phys.* B **24** 1–8
[22] Lateef Al-Badri K S, Abdullah O F and Turki A I 2018 Penta-perfect metamaterial absorber for microwave applications *IOP Conf. Ser.: Mater. Sci. Eng.* **454** 012075
[23] Kalraiya S, Chaudhary R K, Gangwar R K and Abdalla M A 2019 Compact quad-band polarization zhohouindependent metamaterial absorber using circular/square metallic ring resonator *Mater. Res. Express* **6** 4–14
[24] Luo H and Cheng Y Z 2018 Ultra-thin dual-band polarization-insensitive and wide-angle perfect metamaterial absorber based on a single circular sector resonator structure *J. Electron. Mater.* **47** 323–328
[25] Duan X, Chen S, Liu W, Cheng H, Li Z and Tian J 2014 Polarization-insensitive and wide-angle broadband nearly perfect absorber by tunable planar metamaterials in the visible regime *J. Opt. (United Kingdom)* **16** 1-7

[26] Cheng Y Z, Nie Y and Gong R Z 2013 Design of a wide-band metamaterial absorber based on fractal frequency selective surface and resistive films *Phys. Scr.* **88** 1-6
[27] Huang X, He X, Guo L, Yi Y, Xiao B and Yang H 2015 Analysis of ultra-broadband metamaterial absorber based on simplified multi-reflection interference theory *J. Opt. (United Kingdom)* **17** 1-8
[28] Zhou Y, Shen Z, Huang X, Wu J, Li Y, Huang S and Yang H 2019 Ultra-wideband water-based metamaterial absorber with temperature insensitivity *Phys. Lett. Sect. A Gen. At. Solid State Phys.* **383** 2739–2743
[29] Shoghi Badr N and Moradi G 2019 Design and analysis of graphene-based THz absorber using multi-layer structure based on increasing profile for conductivity of the graphene layers *Optik (Stuttg).* **198** 163239
[30] Kong X R, Zhang H F, Dao R N and Liu G B 2019 A tunable polarization insensitive ultra-broadband absorber based on the plasma metamaterial *Opt. Commun.* **453** 124435
[31] Li W, Wei J, Wang W, Hu D, Li Y and Guan J 2016 Ferrite-based metamaterial microwave absorber with absorption frequency magnetically tunable in a wide range *Mater. Des.* **110** 27–34
[32] Zhou Z, Chen K, Zhao J, Chen P, Jiang T, Zhu B, Feng Y and Li Y 2017 Metasurface Salisbury screen: achieving ultra-wideband microwave absorption *Opt. Express* **25** 30241-30252
[33] Khuyen B X, Tung B S, Kim Y J, Hwang J S, Kim K W, Rhee J Y, Lam V D, Kim Y H and Lee Y P 2018 Ultra-subwavelength thickness for dual/triple-band metamaterial absorber at very low frequency *Sci. Rep.* **8** 1–9
[34] Khuyen B X, Tung B S, Van Dung N, Yoo Y J, Kim Y J, Kim K W, Lam V D, Yang J G and Lee Y 2015 Size-efficient metamaterial absorber at low frequencies: design, fabrication, and characterization *J. Appl. Phys.* **117** 243105
[35] He L, Shan D, He J, Liu S, Chen Z and Xu H 2019 Low-frequency perfect sandwich meta-absorber based on magnetic metal *Mod. Phys. Lett.* B **33** 16–20
[36] Wang N, Dong X, Zhou W, He C, Jiang W and Hu S 2016 Low-frequency metamaterial absorber with small-size unit cell based on corrugated surface *AIP Adv.* **6** 025205